

RSC Advances



This is an *Accepted Manuscript*, which has been through the Royal Society of Chemistry peer review process and has been accepted for publication.

Accepted Manuscripts are published online shortly after acceptance, before technical editing, formatting and proof reading. Using this free service, authors can make their results available to the community, in citable form, before we publish the edited article. This *Accepted Manuscript* will be replaced by the edited, formatted and paginated article as soon as this is available.

You can find more information about *Accepted Manuscripts* in the [Information for Authors](#).

Please note that technical editing may introduce minor changes to the text and/or graphics, which may alter content. The journal's standard [Terms & Conditions](#) and the [Ethical guidelines](#) still apply. In no event shall the Royal Society of Chemistry be held responsible for any errors or omissions in this *Accepted Manuscript* or any consequences arising from the use of any information it contains.

ARTICLE

Structure-property relationship of isomeric diphenylethenyl-disubstituted dimethoxycarbazoles

Cite this: DOI: 10.1039/x0xx00000x

Audrius Bucinskas,^a Gintautas Bagdziunas,^a Ausra Tomkeviciene,^a Dmytro Volynyuk,^a Nataliya Kostiv,^a Dalius Gudeika,^a Vygintas Jankauskas,^b Martins Rutkis,^c and Juozas V. Grazulevicius*^a

Received 00th January 2012,
Accepted 00th January 2012

DOI: 10.1039/x0xx00000x

www.rsc.org/

Isomeric 3,6-dimethoxy- and 2,7-dimethoxycarbazoles containing diphenylethenyl moieties were synthesized by condensation of the appropriate dimethoxycarbazoles with diphenylacetaldehyde. The solid-state structures and the molecular order of the compounds were proven by X-ray crystallography. Both compounds were found to be capable of glass formation with the comparable glass transition temperatures (70–71 °C). They exhibited high thermal stabilities, with the 5 % weight loss temperatures exceeding 375 °C. The isomer having diphenylethenyl groups at C-3 and C-6 positions and methoxy groups at C-2 and C-7 positions (**3a**) exhibited aggregation-induced emission (AIE), while its counterpart having diphenylethenyl groups at C-2 and C-7 positions and methoxy groups at C-3 and C-6 positions (**3b**) showed the opposite effect, i.e. aggregation-caused quenching (ACQ). The derivative **3b** showed superior charge transporting properties. Time-of-flight hole drift mobilities in its layers approached 10⁻³ cm²/Vs at high electric fields. A comparative theoretical analysis of the compounds was performed using density functional theory (DFT) and time-dependent DFT calculations. They proved more effective π -conjugation in the derivative of 3,6-dimethoxycarbazole (**3b**), which was also observed by UV and fluorescence spectroscopies. The theoretical study revealed relatively low ground state dipole moment of 0.69 D of the isomer **3b**, while its counterpart (**3a**) showed much higher ground state dipole moment of 5.98 D. The difference in polarity was found to have the crucial effect on the molecular arrangement in the crystals and consequently, on the thermal transitions and charge-transporting properties.

Keywords: Carbazole; Charge mobility; DFT; AIE; ACQ; Reorganization energy; Marcus theory; X-ray crystallography.

Introduction

The search for new π -conjugated organic compounds with advanced properties is still the challenge for many laboratories working on the synthesis of organic electroactive materials for optoelectronic applications. Carbazole derivatives have attracted much attention because of their flexible synthesis and wide range of applications, such as organic light-emitting diodes (OLEDs), organic thin-film transistors, solid-state dye-sensitized solar cells.^{1–4} The carbazole moiety can be easily modified via its C-3 and C-6 positions.⁵ There is a substantial number of studies on 3,6-substituted carbazole derivatives and on their optoelectronic applications. Incomparably less research was done on 2,7-substituted carbazole derivatives. The main obstacle until recently was the lack of an efficient synthesis procedure for these compounds. The obstacle disappeared when the convenient synthetic pathways towards 2,7-dihalocarbazoles were reported.^{6,7} Since then ongoing studies of 2,7-disubstituted carbazole compounds revealed substantially higher hole mobilities compared to those of 3,6-disubstituted

counterparts.⁸ In this work we demonstrate the convenient synthetic method of 2,7-diphenylethenyl disubstituted carbazole derivative by the direct reaction of 3,6-dimethoxy substituted carbazole derivative with diphenylacetaldehyde. We also synthesized the isomeric derivative from 2,7-dimethoxy substituted carbazole derivative and performed the comparative study of the properties of the obtained materials by the theoretical and experimental tools.

Diphenylethenyl-disubstituted derivatives of carbazole were earlier prepared by the multi-step synthetic route, the last step of which was Pd-catalyzed Suzuki coupling of diphenylethenyl borolane with the corresponding dibromocarbazole derivatives.^{9,10} They showed good performance as hole-transporting blue emitters in electroluminescent devices.

In some fields of application, such as dye-sensitized solar cells, electrochemically stable hole-transporting materials with low ionization potentials are required. It is known that introduction of methoxy groups into the structures of aromatic amines as well as the attachment of methoxy-substituted

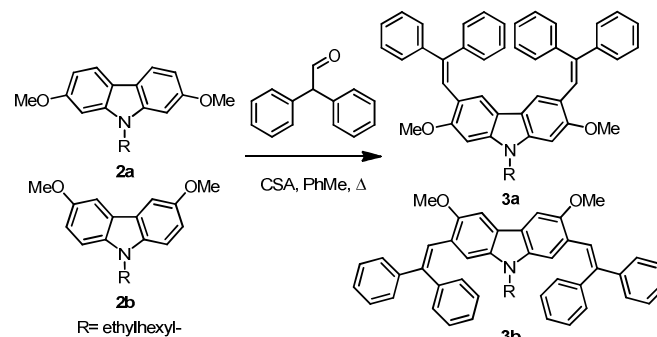
diphenylamino groups to the carbazole moieties lead to the decrease of the ionization potential.^{11,12} The possibility to monitor ionization potentials is also important in the fabrication of OLEDs. The hole-injection barrier differences can strongly affect the efficiency of the devices. The role of the methoxy groups is found to be related to the mesomeric (p-donor) effect and the possibility to establish hydrogen bonds.¹³ The stronger influence was observed for *para*-methoxy substituted derivatives, as compared to *ortho*- and *meta*-methoxy substituted derivatives.^{12,13} The *para*-methoxy substituted derivatives also showed the highest hole mobilities.^{12,13} The effect of the methoxy substitution in carbazole derivatives on their photophysical and photoelectrical properties, to the best of our knowledge, has not yet been studied. Electrochemical and thermal stability is another important property of organic semiconductors. This can lead to the corresponding device degradation.¹⁴⁻¹⁷ It is known that 2,7-substituted derivatives of carbazole show irreversible oxidation with the formation of new carbazolyl derivative.¹⁸ By introducing methoxy or diphenylethenyl groups into C-3 and C-6 positions of carbazole moiety we obtain compounds which demonstrate reversible oxidation and higher electrochemical and thermal stability, in contrast to the non-substituted counterparts.^{8,9}

Results and discussion

Synthesis

Diphenylethenyl-substituted dimethoxycarbazoles (**3a**, **3b**) were synthesized by condensation of the appropriate derivative of dimethoxycarbazole with diphenylacetaldehyde (Scheme 1). This synthetic method of diphenylethenyl-disubstituted derivatives is superior with respect of that reported earlier for the synthesis of the similar derivatives containing no methoxy groups.⁹ It does not

require the preparation of diphenylethenyl borolane and bromination of carbazole.



Scheme 1. Synthesis of **3a** and **3b**.

The starting compound **2a** was prepared by three steps. 2,7-Dimethoxycarbazole (**1a**) was obtained by an Ullmann-coupling followed by a Cadogan cyclization reaction using triphenylphosphine as reported in the literature.^{19,20} Alkylation with 2-ethylhexylbromide was performed by the conventional procedure.²¹ Compound **2b** was synthesized starting from 3,6-dimethoxycarbazole (**1b**) which was prepared by bromination of carbazole with N-bromosuccinimide (NBS) in dimethylformamide (DMF), followed by the direct methoxide displacement of bromine^{22,23} and alkylation by the same procedure as mentioned above. The synthesized compounds were identified by elemental analysis, IR, ¹H and ¹³C NMR, and MS. Compounds **3a**, **3b** were found to be soluble in common organic solvents such as tetrahydrofuran, toluene and chloroform.

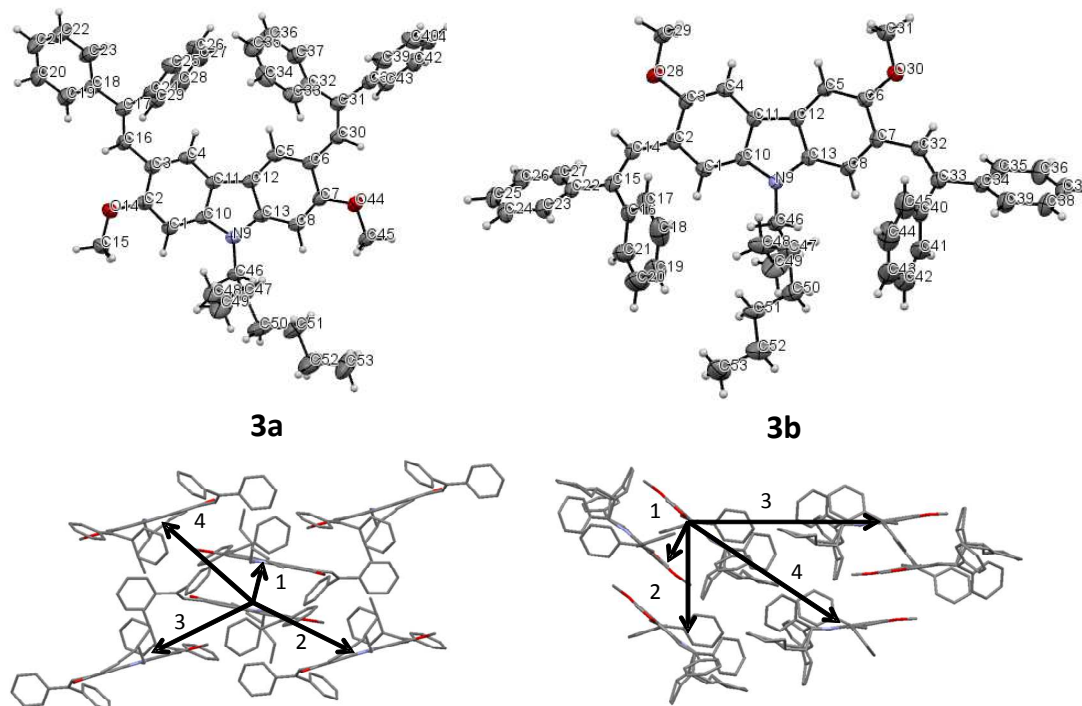


Figure 1. ORTEP diagrams, packing in the crystals and the possible intermolecular charge-hopping channels of **3a-b**.

Crystal structures

According to quantum chemical calculations molecular structures of 2,7-dimethoxycarbazole derivatives (**2a**, **3a**) exhibit relatively high ground state dipole moments (4.53 and 5.98 D, accordingly). At the same time the derivatives of 3,6-dimethoxycarbazole (**2b**, **3b**) are non-polar with low ground state dipole moments (0.30 and 0.69 D). Therefore, one could expect much stronger intermolecular dipole – dipole interaction in case of crystals of **3a** than for **3b**, which in the absence of molecular dipole is built by weaker London dispersion forces. The orpex projections of **3a-b** are shown in Figure 1 and the crystallographic data is listed in Table S1. The racemic compound **3a** crystallizes into the orthorhombic crystal system with space group P-b-c-a. The π -frameworks of **3a** have non-planar geometry and the alkyl chains are extended out of the molecular plane. The analysis of the packing pattern of the molecules of **3a** in the crystalline state revealed that the molecules form columns of alternating opposite interactions, such as C-H \cdots O bonding, which occurs between the enantiomers held together with the different kinds of weak hydrogen atom at C-15 and the oxygen atom O-44 of methoxy groups with the distance of 2.664 Å, C-H \cdots C bonding, which occurs between the hydrogen atom at C-15 and the carbon atom C-45 or between the hydrogen atom at C-53 and the carbon atom C-16 with the distances of 2.712 Å and 2.738 Å, respectively. The distances along the different planes of carbazole rings vary from 3.54 to 3.63 Å. The crystal of **3b** is formed from (*S*)-enantiomer only and is held by C-H \cdots C interactions between the hydrogen atoms at C-29, C-31 and C-49, and carbon atoms C-8, C-6, C-3 and C-10 with the distances of 2.861, 2.899, 2.874 and 2.785 Å, respectively. The C-H \cdots O interactions between the molecules of **3b** was not observed. The angles between ethenyl double bond and the carbazole plane of the molecules **3a** (28.5°, 22.4°) and **3b** (26.1°, 22.5°) were measured. These values were found to be comparable to those of 2-methoxycarbazole 3,6-disubstituted with the diphenylethenyl moieties (30.11°, 23.78°).²⁴

Thermal properties

The thermal properties of the synthesized compounds were estimated by differential scanning calorimetry (DSC) and thermogravimetric analysis (TGA). The thermal characteristics are collected in Table 1. Compounds **3a** and **3b** possess high thermal stability with 5% weight loss temperatures (T_d) of 376 °C and 405 °C, respectively. The DSC measurements showed that **3a** and **3b** are able to form molecular glasses. Compounds **3a** and **3b** were isolated after the synthesis as crystalline substances and their first DSC heating scans revealed endothermal melting signals (Figure 2). Due to the presence of stronger dipole – dipole interactions the crystals of **3a** showed by 25 °C higher melting point than those of **3b**. Compound **3b** exhibited polymorphism which is rather often observed for organic glass forming molecular materials.²⁵

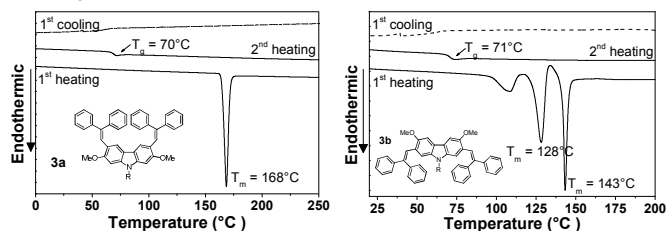


Figure 2. DSC curves of **3a** and **3b** (scan rate 10 °C/min, N₂ atm.).

The ability to form more than one crystal structure could be the result of the weak dipole-dipole interaction between the molecules of **3b**.²⁶ No crystallization was observed during the cooling scans, which indicated the transition from the melt to the glassy state. In the second and the following DSC heating scans **3a** and **3b** exhibited glass transitions at 70 and 71 °C, respectively. This observation shows that the linking topology of **3a-b** has no effect on their glass transition temperatures.

Optical and photophysical properties

The normalized absorption and fluorescence spectra of the dilute solutions in THF and the solid films of **3a** and **3b** are shown in Figure 3. The optical and photophysical characteristics are summarized in Table 1. The absorption maxima of the dilute solutions of **3a** and **3b** were detected at 362 nm and 392 nm, respectively. UV-vis spectrum of **3b** showed considerable bathochromic effect of 30 nm with respect to the spectrum of its counterpart **3a**. These results provide evidence for more effective and prolonged conjugation length in **3b** compared to **3a**.²⁷ Compounds **3a** and **3b** showed emission in a blue and green regions with the emission maxima at 473 and 501 nm, respectively. Fluorescence spectra of **3a** and **3b** exhibited considerable red shifts with respect to those of the starting compounds (**2a** and **2b**, sup. info. Figure S2).

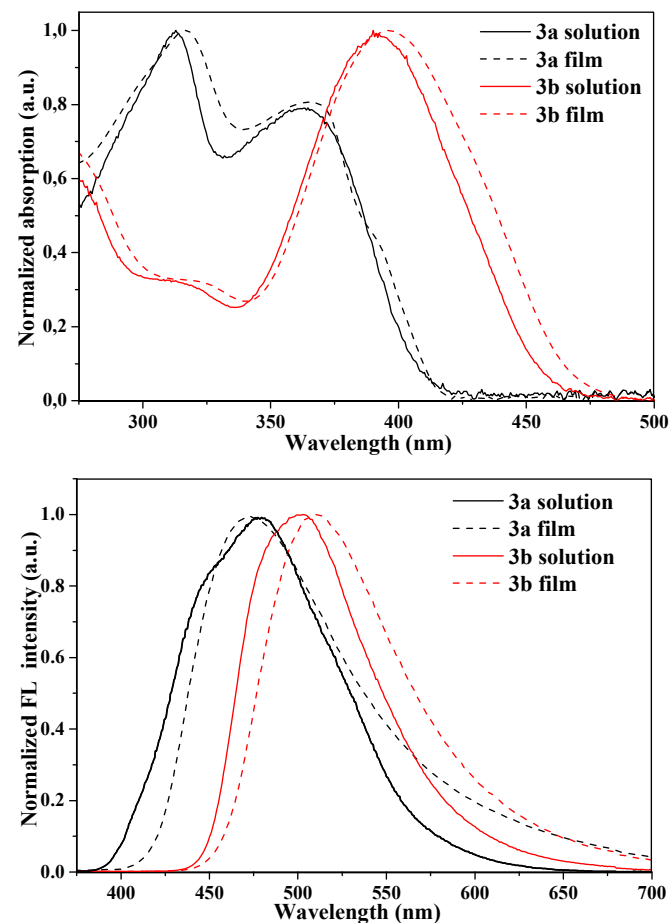


Figure 3. UV-vis and fluorescence spectra of dilute THF solutions (10⁻⁵ M) and of the films of compounds **3a**, **3b**. λ_{ex} = 350 nm.

The target compounds **3a** and **3b** are characterized by long Stokes shifts (~110 nm) which implies that the structures of the emitting state and ground state are rather different. This difference apparently originates from the zwitterionic state of the excited molecules **3a-b**.^{28,29} The absorption and emission spectra of the solvent casted solid amorphous films of **3a** and **3b** were found to be similar to the corresponding spectra of the solutions, but exhibited small red-shifts. Both the solid films and the dilute solutions of **3b** showed higher fluorescence quantum yields as compared to those of **3a**. This observation can be explained by the different zwitterionic states of 3,6-dimethoxy- and 2,7-dimethoxycarbazoles containing diphenylethenyl moieties.⁹ Compound **3a** exhibited the phenomenon of aggregation induced emission which is illustrated by Figure 4a.

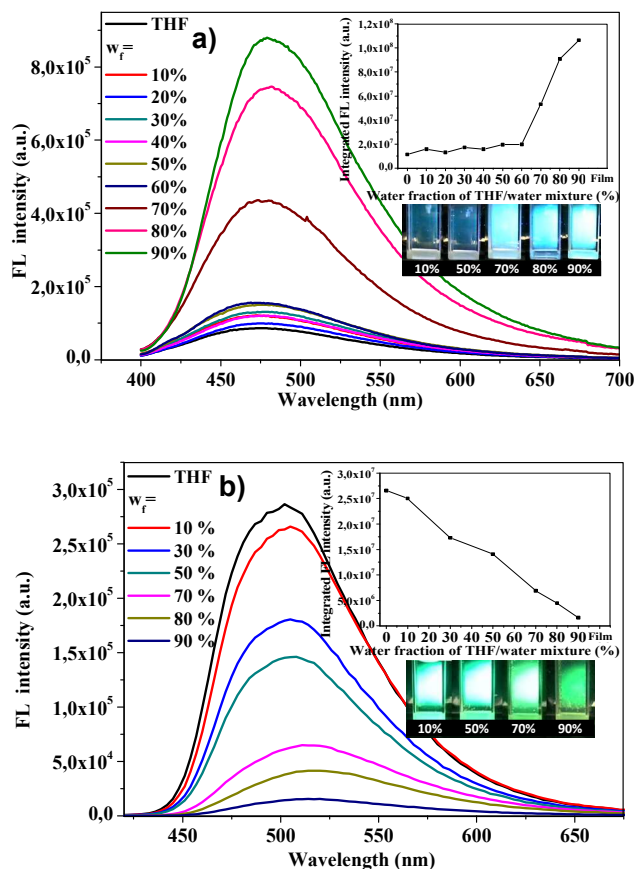


Figure 4. Fluorescence spectra of the dispersions of **3a** (a) and **3b** (b) in water–THF mixtures (10^{-4} – 10^{-5} M). The inset depicts the changes of fluorescence peak intensity. $\lambda_{\text{ex}} = 350$ nm.

The FL intensity of the THF solution was very low and was almost unchanged when water was added up to 60% (v/v), and then started to increase sharply upon further addition of water. These results indicate that the molecules of compound **3a** started to aggregate when the volume fraction of water reached 70%. Clearly, the fluorescence behavior of **3a** is typical of an AIE luminogen.³⁰ The high ground state dipole moment and high dipole-dipole interaction between the molecules of compound **3a** results the restrictions of the molecular motions which can be a key factor explaining the aggregation induced emission.³¹ The X-ray analysis data of **3a** (Figure 1) show that the neighboring dimers, which are arranged parallel but with the opposite induced dipole moments (IDM) of the excited state, can form configuration favorable for the formation of J-aggregates.³² This presumption is confirmed by fluorescence spectroscopy. The intensity maxima of aggregation induced emission are bathochromically shifted by ca. 15 nm compared to the emission maxima of dilute solutions in THF. The totally opposite effect of aggregation-caused quenching was observed for isomer **3b** (Figure 4b). In case of **3b**, the closest dimers are parallel and IDM (Figure 1) are of the opposite direction. However, the ground state dipole moment of **3b** is very small (0.69 D). Therefore IDM is also small and there has no substantial effect on IDM of the surrounding molecules. For this reason no shift in fluorescence spectra was observed and the aggregation induced quenching was monitored. Figure 5 shows fluorescence decay curves of the dilute THF solutions and of the solid films of **3a** and **3b**.

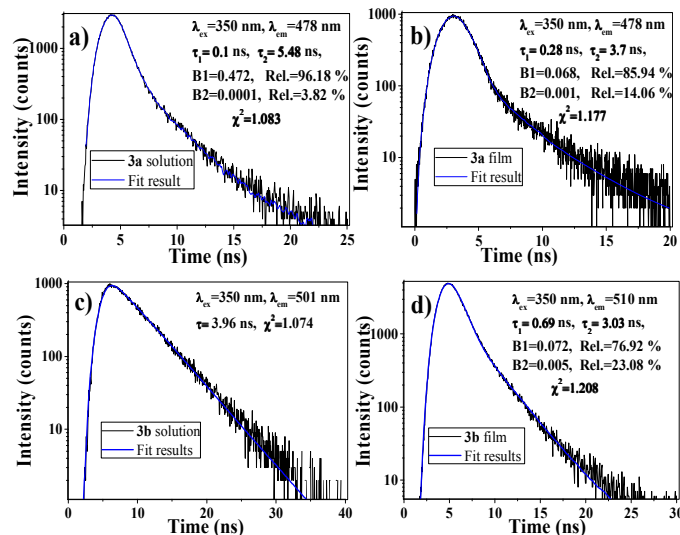


Figure 5. Fluorescence decay curves of the dilute (10–5M) solutions in THF and of the solid films of **3a** (a,b) and **3b** (c,d). Blue lines indicate single or double exponential fits to the experimental data. Fluorescence lifetimes (τ) are indicated.

Table 1. Thermal, optical and photophysical characteristics of compounds **3a** and **3b**.

	$T_m / T_g^a / T_d^b, ^\circ\text{C}$	$\lambda_{\text{max sol}}^{\text{abs}} / \lambda_{\text{max film}}^{\text{abs}}, \text{nm}$	$\lambda_{\text{max sol}}^{\text{em}} / \lambda_{\text{max film}}^{\text{em}}, \text{nm}$	Stokes shift, nm	$\Phi_{\text{sol}} / \Phi_{\text{film}}, \%$	$\tau_{\text{sol}} / \tau_{\text{film}}, \text{ns}$	$\chi_{\text{sol}}^2 / \chi_{\text{c,d film}}^2$	$k_r \text{ sol} / k_r \text{ film}, 10^8 \text{ s}^{-1} \text{ c}$	$k_{nr \text{ sol}} / k_{nr \text{ film}}, 10^8 \text{ s}^{-1} \text{ c}$
3a	168 / 70 / 405	362 / 365	473 / 476	111	1.20 / 2.20	0.10 (96%), 5.48 (4%) / 0.28 (86%), 3.7 (14%)	1.08/1.18	1.2 / 0.8	98.8 / 34.9
3b	128,143 / 71 / 376	392 / 396	501 / 510	109	34.9 / 11.8	3.96 / 0.69(77%), 3.03(23%)	1.07/1.21	0.9 / 1.7	1.6 / 12.8

^a - determined by DSC, scan rate 10 $^\circ\text{C}/\text{min}$, N_2 atmosphere; ^b - 5% weight loss determined by TGA, heating rate 10 $^\circ\text{C}/\text{min}$, N_2 atmosphere; ^c counted for the most prevalent state; ^d the chi-square values show the quality of the fit.

The derivative **3a** exhibited double exponential fluorescence decays originating from two different molecular excited states with the fluorescence life times (τ) of 0.10 and 5.48 ns for the solution and 0.28 ns 3.7 ns for the film with χ^2 ranging from 1.08 to 1.18 respectively. The fluorescence decay of the film of compound **3b** can also be described by the double exponential fit with the fluorescence lifetimes of 0.69 ns and 3.03 ns with χ^2 value of 1.21, while fluorescence decay of the dilute solution of **3b** was adequately described by the single exponential curve with the lifetime of 3.96 ns ($\chi^2 = 1.07$). We presume that the emission with the shorter life time (0.1-0.7 ns) originates from the excited dimethoxycarbazole moiety, while the emission with the longer life time (3.0-5.5 ns) originates from the excited zwitterionic states of **3a-b** derivatives.

To unveil the contributions of the competing radiative and nonradiative relaxation processes, we calculated the radiative (k_r) and nonradiative (k_{nr}) decay rate constants from the singlet excited state using the obtained values of Φ and τ by the following relations: $k_r = \Phi / \tau$, $k_{nr} = (1-\Phi) / \tau$. The results are summarized in Table 1. Interestingly, the calculated k_r and k_{nr} values of **3a-b** were found to be highly dependent on the position of methoxy and diphenylethenyl moieties. For both the isomers **3a-b** the k_r values obtained for the solutions and the solid films showed no any big differences, while the values of k_{nr} observed for the solutions and films of **3a** were found to be significantly higher than those of **3b**. Thus the nonradiative processes are predominant in the relaxation processes of excited states of compound **3a**.

In order to get more insight on the nature of the absorption bands of **3a-b**, TD-DFT calculations were performed. The significant similarities between the theoretical and experimental UV-vis spectra of **3a-b** were observed (Figure 6). The excitation energies and oscillator strengths for the molecules **3a-b** are presented in Table 2.

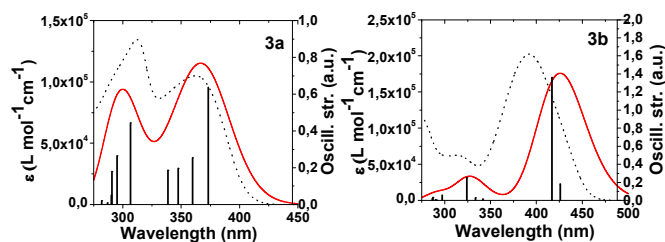


Figure 6. Comparison of the experimental (black-dot) and calculated **3a** and **3b** (red) UV-vis spectra at the B3LYP/6-31G(d,p)/PCM(THF) level ($\sigma = 0.25$ eV); bars represent the oscillator strength.

The lowest energy band for **3a** is influenced by two transitions $S_0 \rightarrow S_1$ and $S_0 \rightarrow S_2$ with the maxima of ϵ at 376 and 362 nm, respectively. The first excitation with the oscillator strength of 0.637 for **3a** corresponds to the HOMO \rightarrow LUMO transition (figure 7). This transition is localized on the diphenylethenyl and dimethoxycarbazole moieties. Therefore, this excitation corresponds to $\pi-\pi^*$ transition for both conjugated chromophores. The absorption band with the maximum at 312 nm of **3a** corresponds to the calculated $S_0 \rightarrow S_5$ and $S_0 \rightarrow S_6$ transitions. The $S_0 \rightarrow S_5$ transition, according to the nomenclature of Platt,³³ is named as 1L_a transition because the orbitals on the carbazole moiety are oriented along the symmetry axis.³⁴

Table 2. Properties of the selected transitions and their contribution to the UV-vis spectra of **3a-b** calculated at the B3LYP/6-31G(d,p)/PCM(THF) level.

	Exp UV λ , nm	Cal UV λ , nm	Tr.	Osc. Stren. a.u.	Contributions (more than 20%)
3a	362	376	1	0.637	H \rightarrow L (95%)
		362	2	0.254	H-1 \rightarrow L (90%)
	312	307	5	0.443	H \rightarrow L+2 (77%)
		296	6	0.265	H-1 \rightarrow L+2 (63%)
3b	392	434	1	0.181	H \rightarrow L (63%), H-1 \rightarrow L (35%)
		425	2	1.363	H \rightarrow L (35%), H-1 \rightarrow L (63%)
	317	327	5	0.253	H-2 \rightarrow L (67%)

The absorption band with the similar wavelength for *N*-substituted 2,7-dimethoxycarbazole was observed experimentally.³⁵ Therefore, these excitations are assigned to $\pi-\pi^*$ transition in the dimethoxycarbazole moiety.

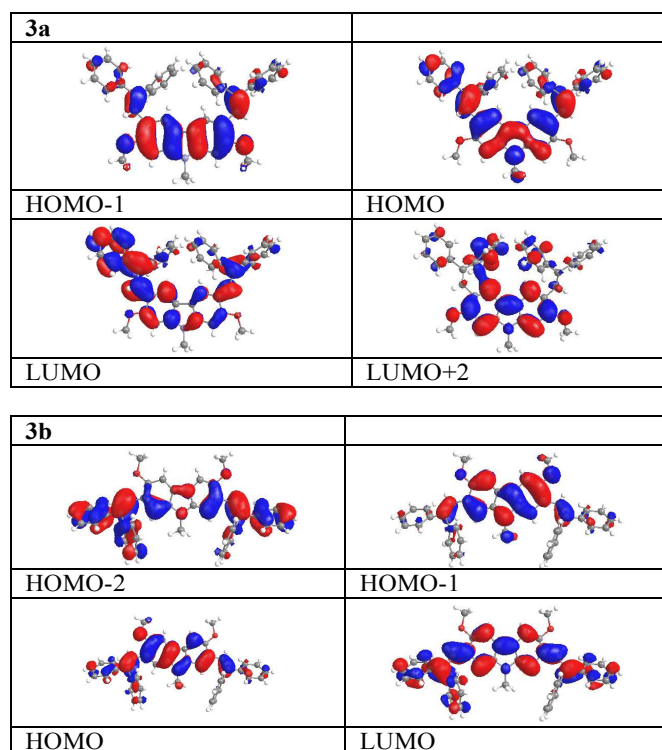


Figure 7. The computed spatial distributions of HOMO and LUMO orbitals for **3a** and **3b**.

The situation with **3b** was found to be different. The lowest energy absorption band of **3b** is influenced by two lower energy transitions compared to those of **3a**, i.e. $S_0 \rightarrow S_1$ and $S_0 \rightarrow S_2$ transitions which manifest themselves at 434 and 425 nm, respectively. The attachment of methoxy groups at C-3 and C-6 positions of the carbazole ring generates the intramolecular charge transfer (ICT) from carbazole to diphenylethenyl moieties which subsequently results in the zwitterionic state. A positive charge is delocalized on C-3 or C-6 positions of the carbazole moiety and a negative charge is on diphenylethenyl moiety. The first $S_0 \rightarrow S_1$ excitation with the oscillator strength

of 0.181 a.u. of **3b** corresponds to the HOMO→LUMO and HOMO-1→LUMO transitions with 63 and 35 % contributions, respectively (figure 7). This excitation is a mixture of the π - π^* transitions of both conjugated chromophores and ICT transition from carbazole to diphenylethenyl moieties. In other words, $S_0 \rightarrow S_1$ can be regarded as zwitterionic transition in nature⁹. The electron density in the carbazole ring is delocalized symmetrically because of the ICT transition. The second $S_0 \rightarrow S_2$ excitation at 425 nm corresponds to the same $S_0 \rightarrow S_1$ transition, but the orbital contributions are 35 and 63 %, respectively. Similarly, this excitation is a mixture of the π - π^* transition of both conjugated chromophores and ICT transition from the carbazole to the diphenylethenyl moiety. The obtained oscillator strength (0.181 a.u.) of the first excitation of **3b** is lower than that of **3a**. The UV absorption band at 317 nm is influenced by $S_0 \rightarrow S_5$ excitation which corresponds to the HOMO-2→LUMO transition. This $S_0 \rightarrow S_5$ excitation is the mixture of π - π^* transitions in the diphenylethenyl and carbazole chromophores.

The energies of HOMO and LUMO of **3a-b** were calculated using the same method as for UV-vis spectra. The energies of HOMO and LUMO for **3a** were found to be -4.97 eV and -1.16 eV, respectively, and those observed for **3b** were -4.93 eV and -1.60 eV, respectively. The calculated HOMO energy levels are in good agreement with the experimental values (Table 3).

Electrochemical properties and ionization potentials

Electrochemical properties of the solutions of the compounds in dichloromethane with 0.1 M tetrabutylammonium hexafluorophosphate as supporting electrolyte were studied by the cyclic voltammetry (CV) using Ag/AgNO₃ as the reference electrode and a Pt wire counter electrode. The electrochemical characteristics are summarized in Table 3. The CV curves of **3a-b** are shown in Figure 8.

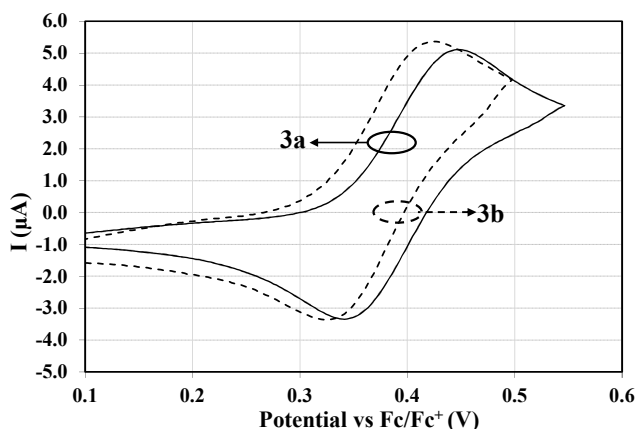


Figure 8. Cyclic voltammograms of **3a-b** at 10^{-3} mol L⁻¹ in a solution of argon-purged TBAP (0.1M) in CH₂Cl₂. $\nu = 50$ mV/s.

No reduction waves was observed down to ca -1.5 V in CV curves of all the studied compounds. However, all the compounds showed the oxidation waves up to ca 0.31 V. The oxidation was found to be irreversible only for compound **2a** (Figure S2), having unsubstituted C-3 and C-6 positions of carbazole ring. It was found to be quasi-reversible for **2b**. Irreversible oxidation of **2a** was followed by coupling of carbazole radical cations because of higher electron spin density at C-3 and C-6 positions³⁷ and formation of new carbazolyil-containing compounds.¹⁸

The oxidation of **3a** and **3b** was found to be reversible up to ca 0.55 V. Precursor **2b** and compounds **3a-b** showed oxidation peaks at 0.51V, 0.45V and 0.43V, respectively, and after five repeated oxidation and reduction cycles their CV curves did not change. The oxidation of compound **2a** started at 0.41 V and, subsequently, the oxidation peak at 0.53 V was observed. The HOMO energy levels were determined using the relationship $E_{\text{HOMO}}(\text{eV}) = -1.4E_{\text{onset,ox}}(\text{V}) - 4.6$.³⁸ The HOMO energy levels of the derivatives **3a** and **3b** were found to be comparable and a little higher with respect to those of compounds **2a-b**.

Table 3. Electrochemical characteristics of **3a**, **3b** and **2a**, **2b**.

	$E_{\text{onset}}^{\text{a}}$, V	$E_{\text{ox}}^{\text{pa}}$, V	$E_{\text{ox}}^{\text{pc}}$, V	$\frac{E_{\text{HOMO}}^{\text{DFT}}}{E_{\text{HOMO}}}$, eV	E_{g} , eV	IP, eV
2a	0.41	0.53	- ^f	-5.17 / -	3.69	5.68
2b	0.35	0.51	0.33	-5.09 / -	3.16	5.50
3a	0.33	0.45	0.35	-5.06 / -4.97	3.05	5.38
3b	0.31	0.43	0.33	-5.03 / -4.93	2.72	5.41

^a Onset, oxidation and reduction potentials vs Fc. ^c $E_{\text{HOMO}}(\text{eV}) = -1.4E_{\text{onset,ox}}(\text{V}) - 4.6$, where $E_{\text{onset,ox}}$ was determined by solution-based cyclic voltammetry.³⁶ ^d The optical bandgap energies estimated from the absorption edges. ^e Ionization energy (IP) for the solid films was measured by the electron photoemission in air method. ^f Irreversible oxidation.

The HOMO levels acquired from the DFT calculations and from CV measurements were found to be in good agreement for compounds **3a-b** and showed higher values compared to the diphenylethenyl-substituted derivatives of carbazole containing no methoxy groups.⁹

The ionization potentials (IP) of the synthesized compounds were measured by the electron photoemission in air technique. The results are presented in Table 3. Usually the photoemission experiments are carried out in vacuum but, in our case, the investigated organic compounds were stable with respect to oxygen and the measurements could be carried out in air. All the synthesized compounds showed lower IP values compared to compounds containing electronically isolated carbazole moieties having no substituents at the aromatic rings.³⁹ Methoxy-disubstituted carbazoles (**2a,b**) showed a little higher IP than the target compounds (**3a,b**). Compounds **3a** and **3b** were found to exhibit the comparable IP values. This observation proves our earlier finding that the alteration of the substitution patterns of carbazole moiety practically does not affect the ionization energy values.⁸

Charge-transporting properties

The hole-transporting properties of the layers of compounds **3a** and **3b** were studied by the xerographic time-of-flight (XTOF) and the time of flight (TOF) techniques. The sample of compound **3b** for the XTOF measurements was prepared by drop casting technique with the layer thickness of ca. 2.5 μm . Because of high disposition to crystallization it was not possible to obtain good quality amorphous film of compound **3a** using the same film preparation method. The value of hole drift mobilities of the layer **3b** was found to be 4.1×10^{-3} cm²/Vs at electric field of 1.23×10^6 V/cm. Figure 9a shows hole photocurrent transients on log-log and linear (insets) scales that were observed for the layer of **3b**. No transit times were detect-

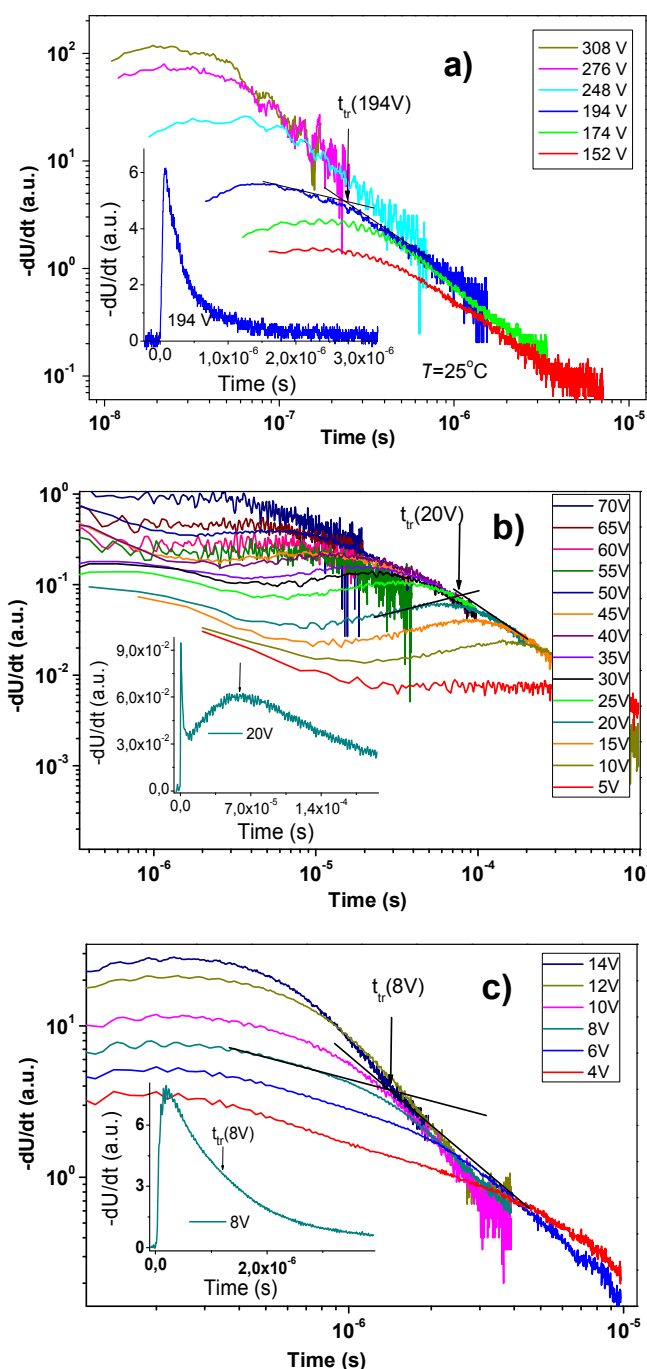


Figure 9. XTOF transients for the drop-casted layer of **3b** (a) and TOF transients for the vacuum deposited layers of **3a** (b) and **3b** (c). The insets show transient curves in the linear plot.

ed in the linear plots, however, they were seen on log-log plots. This observation shows that dispersive hole transport is characteristic of the layer of **3b**. Hole-transporting properties of compounds **3a** and **3b** were also investigated by the TOF technique using the vacuum deposited amorphous layers. The layer thickness was in the range of 0.65–2.8 μm . Figures 9b–c show the hole photocurrent transients of **3a** and **3b** on log-log and linear (insets) scales. The different character of the transients is obvious. Compound **3a** showed low dispersion hole transport, while compound **3b** demonstrated high dispersion transport.

Figure 10 shows the electric field dependencies of hole-drift mobility values (μ) for the layers of **3a** and **3b**. The logarithm of the hole-drift mobility values showed linear dependencies on the square root of the electric field. The similar characteristic dependencies were observed for many amorphous (disordered) organic semiconductors and were explained in terms of the Bassler and Borsenberger model.⁴⁰ The zero field hole drift mobility (μ_0) and the field dependence parameter (α) was obtained by the extrapolation of the electric-field dependencies of the hole drift mobilities to the zero electric field (Figure 10, Table 4):

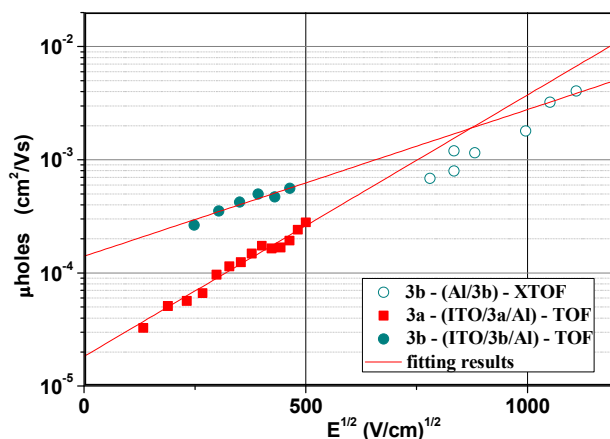


Figure 10. Electric field dependencies of hole mobilities in the layers of **3a** and **3b**.

Table 4. The hole mobility data for compounds **3a** and **3b**.

	$\mu_0 / \mu_0^{\text{theor}}$, cm^2/Vs	μ_i , cm^2/Vs^a	α , 10^{-3} cm/V
3a	$1.8 \times 10^{-5} / 7.7 \times 10^{-6}$	2.6×10^{-4}	5.3
3b	$1.4 \times 10^{-4} / 1.5 \times 10^{-4}$	6.2×10^{-4}	4.6

^a mobility value at an electric field of 2.5×10^5 V/cm

Compound **3b** showed higher hole mobility and a little lower field dependence parameter than **3a**.

To get deeper insight into the hole-transporting properties of the isomers **3a–b** the theoretical calculations were performed. The crystal structure to the large extent determines the charge carrier transport pathways and charge mobilities in organic molecular crystals.⁴¹ For some compounds the mesoscopically connected networks in the amorphous films are possible even without a periodic order.⁴²

In this work, the crystal structures of **3a–b** were used to generate a wide variety of possible hopping pathways (dimers) showed in Figure 1 and Figure S4. According to the Holstein small polaron limit, the charge is localized on a single organic molecule. The standard Marcus-Hush model (1) describes the rate of charge transfer between molecules:⁴³

$$k_i = \frac{2\pi}{\hbar} |H_i|^2 \frac{1}{\sqrt{4\pi\lambda k_b T}} \exp\left(-\frac{(\lambda + \Delta G^0)^2}{4\lambda k_b T}\right) \quad (1)$$

where k_i is the electron transfer rate constant for pathway i , H_i is the electronic coupling between the initial and final states, λ is the reorganization energy ($\lambda = \lambda_{\text{in}} + \lambda_{\text{out}}$, i.e. the sum of both inner and outer-sphere), ΔG^0 is the total Gibbs free energy change for the electron transfer reaction, k_b is the Boltzmann constant and T is the absolute temperature (298 K).

Many theoretical and experimental studies concerning λ of single molecules were reported.⁴⁴ However, relevant for charge mobility is the charge reorganization energy of organic solids.

The charge reorganization energy is the sum of inter- and intramolecular effects, where the intramolecular effects dominate the charge-phonon coupling. However, their energy is very small (10-100 meV) and the crucial point to access the impact to charge mobility in the solid state is not performed.⁴⁵ The other factor is a charge carrier polarization energy. The polarization energy is significant for the organic materials and ranges between -0.1 eV and -1.0 eV.⁴⁶ The polarization energy (P^+ and P^-) measures the contribution from intermolecular interactions in the crystal to hole and electron transport levels and includes both an electrostatic and a polarization contribution.⁴⁷ P^+ energy is defined as the difference between the solid state and gas phase values of ionization potential.⁴⁸ We assume that the Gibbs free energy (ΔG^0) is approximately equal to the polarization energy for one dimension of the crystal for holes and can be described as $\Delta G^0 \approx -\frac{1}{3}P^+$. The P^+ energy can be estimated theoretically from the stand-alone molecule ionization potential (IP) (it can be obtained from vertical IP calculation in vacuum) and the IP of the solid state (it can be obtained from vertical IP calculation in one crystal lattice) using the formula $P^+ = IP_{\text{solid}} - IP_{\text{vacuum}}$. The calculated P^+ energy values were found to be -0.69 eV for **3a** and -0.57 eV for **3b**.

The internal reorganization energy (λ_{in}) values were calculated using the normal-mode analysis method.⁴⁹ This value for the model compound was calculated at the B3LYP/6-311+G(d,p) level in vacuum according to the following equation:

$$\lambda_{\text{in}} = [E^\pm(g^0) - E^\pm(g^\pm)] + [E^0(g^\pm) - E^0(g^0)] \quad (2)$$

In this equation, E corresponds to the energy of the neutral molecule (g^0) in the geometry of the cationic/anionic species (g^\pm). The reorganization energies of **3a** and **3b** for holes (λ_+) were found to be 0.32 and 0.26 eV, and for electrons (λ_-) they were found to be 0.31 and 0.36 eV. These results show that the reorganization energies for holes and electrons of **3a-b** are somewhat similar.

The electronic coupling (transfer) integrals H_i for the pathways (see Figure 1) were estimated using the energy splitting in dimmer method⁵⁰ (3) at the long-range corrected hybrid density functional wB97X-D⁵¹ and 6-31G(d) basis set using the Spartan'14 package⁵² in vacuum:

$$H_i = \frac{E_{L+1(H)} - E_{L(H-1)}}{2} \quad (3)$$

where $E_{L[H]}$ and $E_{L+1[H-1]}$ are the energies of the LUMO and LUMO+1 (HOMO and HOMO-1) levels taken from the neutral state from the crystal structures of **3a-b**. The molecules in the crystal structures were not optimized. The 2-ethylhexyl chains were approximated by methyl groups to reduce computational time for the calculation of the reorganization energies and the electronic coupling integrals.

The diffusion coefficient (D) for migration of electrons or holes in the dimmers is given by the equation (4):⁵³

$$D = \frac{1}{2N} \frac{\sum d_i^2 k_i^2}{\sum k_i} \quad (4)$$

where N is the dimensionality of the crystal ($N=3$) and d_i is the distance between the dimmers mass centers. Then, according to the Einstein equation (5), the final drift mobility (μ_0) in the absence of electric field was calculated using the single-step approximation:

$$\mu_0 = \frac{e \cdot D}{k_b T} \quad (5)$$

where e is the electron charge, $T=298$ K.

The electronic coupling (transfer) integrals are very sensitive to the relative positions of molecules in the solid state.⁵⁰ The electronic couplings were evaluated using the dimmer model. Here, the single-crystal structures of **3a-b** were used to generate a wide variety of possible intermolecular charge-hopping channels (transport pathways shown in Figure 1 and Figure S4). The distances between molecular mass centers and charge transfer integrals for all hopping pathways are listed in Table 5:

Table 5. The data of the theoretical calculation of hole mobility at 298 K.

Dimension (N=1) for 3a	d, Å	Angle, deg. ^a	H _h , meV	k _h , 10 ⁸ s ⁻¹ for holes	μ _{0 h} , 10 ⁻⁵ cm ² /Vs
1	3.58	180	59	3.94	0.98
2	10.4	163	42	2.01	4.22
3	14.6	48	34	1.29	5.39
4	15.8	77	32	1.18	5.72
3a	D _h , 10 ⁻⁶ cm ² /s		μ _{0 h} , 10 ⁻⁶ cm ² /s/V		
N=3	0.25		7.65		
Dimension (N=1) for 3b	d, Å	Angle, deg. ^a	H _h , meV	k _h , 10 ⁷ s ⁻¹ for hole	μ _{0 h} , 10 ⁻⁵ cm ² /Vs
1	6.00	180	110	672	47.1
2	11.5	122	11	5.79	1.49
3	17.2	58	31	47.7	27.4
4	22.7	180	0.2	0.002	0.0047
3b	D _h , 10 ⁻⁶ cm ² /s		μ _{0 h} , 10 ⁻⁴ cm ² /s/V		
N=3	3.89		1.51		

^a the torsions angle between dipoles of the ¹L_a transition of carbazole moiety in dimmers.

The molecules of compound **3a** in the channels 1 and 2 exhibit the close face-to-face stacking arrangement with the short interplanar distance of ca 3.6 Å. This stacked fashion has provided high electronic coupling reaching 59 and 42 meV for holes. The channel 1 is not dominant in the charge carrier mobility between the molecules (Figure 1, Table 5). The higher charge carrier mobilities were estimated for channels 2-4. This theoretical observation demonstrates that the orientation of dimmers is very important for charge carrier mobility. The orientation of dimmers was estimated from the torsion angle between dipoles of ¹L_a transition in carbazole moiety. This transition dipole is parallel to the N-C(alkyl) bond and is located on the carbazole moiety. The transition dipoles of molecules **3a** in channel 1 are parallel but with the opposite directions (Figure 1, figure S4). Taking into account the distances between dimmers, the molecular orientation has a crucial role in charge carrier mobility. This effect is even clearer in the case of compound **3b**. The higher hole mobility was estimated for the channel 1 as compared with 2-4 channels. The transition dipoles of molecules **3b** in channel 1 are parallel and with the same directions. These observations are well in line with the exciton coupling model in molecular spectroscopy.⁵⁴ In other words, the excitonic coupling between the molecules plays a crucial role in charge carrier mobility. The calculated charge carrier mobilities are in good agreement with the experimental data (Table 4). Considering the different polarity we can explain the different charge carrier mobilities of the target compounds **3a-b**. According to some authors,^{55,56}

higher induced dipole moment may cause lower charge mobility.

Experimental

Instrumentation

^1H and ^{13}C NMR spectra were recorded using Varian Unity Inova (300 MHz (^1H), 75.4 MHz (^{13}C)) and Bruker Avance III 400 spectrometer (400 MHz (^1H), 100 MHz (^{13}C)) apparatus. Chemical shifts (δ) are reported in parts per million (ppm) referenced to tetramethylsilane or internal (NMR) solvent signal. Infrared (IR) spectra were recorded on Perkin Elmer Spectrum GX spectrometer. The spectra of the solid compounds were recorded using KBr pellets. Mass (MS) spectra were obtained on Bruker maxis 4G. Elemental analysis was performed with an Exeter Analytical CE-440 Elemental. Melting points (m.p.) of the synthesized compounds were estimated using Electrothermal Mel-Temp apparatus. Elemental analysis was performed with an Exeter Analytical CE-440 Elemental.

For X-ray crystallography analysis diffraction data were collected on a Bruker-Nonius Kappa CCD single diffractometer using graphite monochromated Mo-K α radiation ($\lambda = 0.71073 \text{ \AA}$). The crystal structure was solved by direct methods [SIR-97] and refined by full-matrix least squares [SHELXL-97]. Mercury 3.3 software⁵⁷ was used for molecular graphics.

UV spectra were recorded with Aventes AvaSpec-2048XL spectrometer. Fluorescence (FL) spectra and fluorescence decay curves of the dilute THF solutions and of the solid films of the compounds were recorded by Edinburgh Instruments FLS980 spectrometer. Fluorescence quantum yields were measured using integrated sphere calibrated with two standards: quinine sulfate in 0.1 M H $_2$ SO $_4$ and rhodamine 6G in ethanol.

DSC measurements were carried out in a nitrogen atmosphere with a Perkin Elmer at DSC 8500 equipment at heating rate of 10 $^\circ\text{C}/\text{min}$. TGA was performed on a Perkin Elmer TGA 4000 apparatus in a nitrogen atmosphere at a heating rate of 10 $^\circ\text{C}/\text{min}$.

Cyclic voltammetry measurements were carried out by a three-electrode assembly cell from a Bio-Logic SAS and a micro-AUTOLAB Type III potentiostat-galvanostat. The measurements were carried out with a glassy carbon electrode in dichloromethane solutions containing 0.1 M tetrabutylammonium hexafluorophosphate as electrolyte, Ag/AgNO $_3$ as the reference electrode, and a Pt wire counter electrode.

The ionization energies of the films of the synthesized compounds were measured by an electron photoemission in air method as described before.⁵⁸ The samples for the measurements were prepared by dissolving materials in THF and by coating on Al plates pre-coated with ca. 0.5 μm thick methylmethacrylate and methacrylic acid copolymer adhesive layer.⁵⁹ The measurement method was, in principle, similar to the described in literature.⁶⁰

The charge transport properties of the drop-casted thin amorphous layer of the materials were investigated by xerographic time-of-flight (XTOF) method using the experimental setup described in literature.^{61,62} Furthermore, the charge carrier mobility (μ) measurements of the vacuum deposited layers of target materials were carried out by the time of flight method.⁶³ The sandwich-like samples (ITO/compounds/Al) were used for the measurements. The layers of materials were prepared on precleaned ITO-coated glass substrates from Sigma-Aldrich with a sheet resistance of 70-100 Ω/sq . Then Al electrodes were evaporated at a pressure below 5×10^{-5} mbar. ITO-coated glass substrates were cleaned by successive washing with deionized water, THF, and trichloroethene in an

ultrasonic bath. Each operation lasted over 5 minutes. The deposition rates of materials and Al were 0.2–0.3 $\text{\AA}/\text{s}$ and $\sim 15 \text{ \AA}/\text{s}$, respectively. The thicknesses of the films of target compounds vary from 0.65 to 2.5 μm , respectively, and active area of that obtained samples was 6 mm^2 . The layers were undertaken by exciting materials through the ITO layer. The charge carriers were generated at the layer surface by illumination with a Nd:YAG laser EKSPALA NL300 (pulse duration was 3–6 ns, wavelength 355 nm). The total photogenerated charge was kept small enough to avoid space charge effects. The electronic time response of the measurement circuit ($\tau = RC$) was always selected to be smaller than the transit time ($\tau \ll t_{tr}$). The transit time was determined from the kink point in the transient photocurrent curves. The transit time t_{tr} with the applied bias (V) indicates the passage of holes through the entire thickness of the cell (d) and enables determination of the hole mobility as $\mu = d^2/U \times t_{tr}$. The experimental setup consisted of a delay generator Tektronix AFG 3102C and a digital storage oscilloscope Tektronix TDS 3032C.

Computational details

Time dependent density function (TD-DFT) calculations of UV-vis spectra of **3a-b** were performed with the Gaussian 09 software package.⁶⁴ The geometries of the molecules of **3a** and **3b** were optimized from X-ray data as the starting point using B3LYP functional and 6-31G(d,p) basis set, followed by calculations of their harmonic vibrational frequencies to verify their stability. All the calculated vibrational frequencies are real, which indicates the true minimum of the total energy on the potential energy hypersurface. The alkyl chains were approximated by methyl groups to reduce the computational time. The simulations were performed for THF solutions using a polarizable continuum model (IEFPCM) to assess the influence of the solvent polarity onto the molecular vertical excitation energies. The half-width at 1/e of the peak maximum σ value of 0.25 eV was used in this work. Up to 10 lowest energies of the excited states were calculated.

Materials

Carbazole, N-bromosuccinimide, chloroform, potassium hydroxide, copper(I) iodide, dry methanol, dry dimethylformamide (DMF), sodium, 2-ethylhexylbromide, potassium carbonate, acetone, diphenylacetaldehyde, (rac)-camphor-10-sulfonic acid (CSA) were purchased from Aldrich and used as received without further purification.

2,7-Dimethoxycarbazole (1a), FW=227 g/mol, m.p.: 270–272 $^\circ\text{C}$, lit.: 272–274 $^\circ\text{C}$) was achieved by an Ullmann-coupling and a Cadogan cyclization as reported in the literature.^{19,20} ^1H NMR (400 MHz, DMSO) δ 10.98 (s, 1H), 7.83 (d, $J = 8.5 \text{ Hz}$, 2H), 6.93 (d, $J = 2.2 \text{ Hz}$, 2H), 6.72 (dd, $J = 8.5, 2.3 \text{ Hz}$, 2H), 3.82 (s, 6H). ^{13}C NMR (101 MHz, DMSO) δ 157.6, 141.0, 120.0, 116.5, 107.3, 94.7, 55.2. **3,6-Dimethoxycarbazole (1b)**, FW=227 g/mol, m.p.: 130–131 $^\circ\text{C}$, lit.: 131–133 $^\circ\text{C}$) was prepared by bromination and methoxylation reactions by the procedures described in literature.^{22,23} ^1H NMR (300 MHz, CDCl $_3$) δ 7.74 (s, 1H), 7.49 (d, $J = 2.5 \text{ Hz}$, 2H), 7.22 (dd, $J = 8.8, 0.5 \text{ Hz}$, 2H), 7.03 (dd, $J = 8.8, 2.5 \text{ Hz}$, 2H), 3.91 (s, 6H). ^{13}C NMR (75 MHz, CDCl $_3$) δ 153.7, 135.4, 123.8, 115.3, 111.7, 102.94, 56.2.

9-(2-Ethylhexyl)-2,7-dimethoxycarbazole (2a) was prepared by the reaction of 2,7-dimethoxycarbazole with an excess of 2-ethylhexylbromide under the basic conditions in the presence of a phase transfer catalyst. 2,7-Dimethoxycarbazole (**1a**, 0.40 g, 1.8 mmol), 2-ethylhexylbromide (0.38 g, 2.1 mmol), potassium carbonate (0.10 g, 0.70 mmol), potassium hydroxide (0.30 g, 5.3 mmol) and catalytic amount of tetrabutylammonium hydrogensulfate were refluxed (2 h) in acetone (14 ml). After TLC (acetone/hexane,

1:10) control, when the starting compound **1a** disappeared, the reaction was terminated, cooled down to the room temperature, treated with ethyl acetate and washed with distilled water. The organic layer was dried over anhydrous Na₂SO₄, filtered and the solvents were removed. The residue was purified by silica-gel column chromatography using the mixture of hexane and acetone (20:1) as the eluent. The yield of yellowish crystals was 75 % (0.45 g, FW = 339 g/mol, m.p.: 86–88 °C). ¹H NMR (400 MHz, CDCl₃) δ 7.77 (dd, *J* = 7.9, 1.0 Hz, 2H), 6.75 – 6.72 (m, 4H), 3.99 – 3.92 (m, 2H), 3.84 (s, 6H), 2.00 – 1.93 (m, 1H), 1.33 – 1.18 (m, 8H), 0.84 (t, *J* = 7.4 Hz, 3H), 0.80 (t, *J* = 7.2 Hz, 3H). ¹³C NMR (75 MHz, CDCl₃, δ, ppm): 158.0, 142.4, 120.0, 116.9, 106.5, 93.8, 55.6, 47.3, 39.1, 30.9, 28.8, 24.4, 23.0, 14.0, 10.9.

9-(2-Ethylhexyl)-3,6-dimethoxycarbazole (2b) was synthesized by the similar procedure as compound **2a** using 3,6-dimethoxycarbazole (**1b**, 0.5 g, 2.2 mmol), 2-ethylhexylbromide (0.51 g, 2.6 mmol), potassium carbonate (0.12 g, 0.88 mmol), potassium hydroxide (0.37 g, 6.6 mmol), catalytic amount of tetrabutylammonium hydrogensulfate and 15 ml of acetone. The yield was 77 % (0.58 g) of s yellowish oil. ¹H NMR (300 MHz, CDCl₃, δ, ppm): 7.50 (s, 2H, Ar), 7.23 (d, *J* = 8.9 Hz, 2H, Ar), 7.05 (dd, *J*₁ = 8.9 Hz, *J*₂ = 2.5 Hz, 2H), 4.05 (d, *J* = 7.4 Hz, 2H, NCH₂), 3.90 (s, 6H, OCH₃), 2.02–1.93 (m, 1H, CH), 1.33–1.19 (m, 8H, CH₂), 0.86 (t, *J* = 7.4 Hz, 3H, CH₃), 0.83 (t, *J* = 7.3 Hz, 3H, CH₃). ¹³C NMR (75 MHz, CDCl₃, δ, ppm): 153.0, 136.5, 122.6, 114.9, 109.7, 102.8, 56.0, 47.5, 39.5, 30.9, 28.8, 24.3, 23.0, 14.0, 10.9.

3,6-Bis(2,2-diphenylethenyl)-9-(2-ethylhexyl)-2,7-dimethoxycarbazole (3a). 9-(2-ethylhexyl)-2,7-dimethoxy-carbazole (**2a**, 0.37 g, 1.08 mmol), diphenylacetaldehyde (0.46 g, 2.37 mmol) were dissolved in toluene (5 ml) at a reflux temperature and catalyzed by CSA (0.30 g, 1.29 mmol). Water generated during the course of the reaction (8 h) was removed by Dean–Stark trap. After TLC control (ethyl acetate/hexane, 1:10), when the starting compound **2a** disappeared, the reaction was terminated, cooled down to the room temperature, treated with ethyl acetate and washed with distilled water. The organic layer was dried over anhydrous Na₂SO₄, filtered and concentrated under vacuum. The residue was purified by silica-gel column chromatography using the mixture of hexane and ethyl acetate (20:1) as the eluent and recrystallized from the mixture of hexane and ethylacetate. The yield of yellow crystals was 35 % (0.26 g, FW = 695 g/mol, m.p.: 166–167 °C). ¹H NMR (300 MHz, CDCl₃) δ 7.38 – 7.17 (m, 22H), 6.89 (s, 2H), 6.65 (s, 2H), 3.97 – 3.94 (m, 2H), 3.86 (s, 6H), 2.01 – 1.94 (m, 1H), 1.39 – 1.25 (m, 8H), 0.98 – 0.86 (m, 6H). ¹³C NMR (75 MHz, CDCl₃, δ, ppm): 156.7, 144.3, 141.3, 141.2, 140.5, 130.6, 128.5, 128.2, 127.9, 127.0 (127.0), 124.0, 120.9, 119.2, 116.2, 91.2, 55.9, 47.3, 39.4, 31.1, 29.0, 27.1, 24.6, 23.2, 14.2, 11.1. *v*_{max} (KBr): 3080, 3051, 3024 (arene C–H, 3100–3000 cm⁻¹); 2959, 2924, 2872, 2855 (aliphatic C–H, 3000–2850 cm⁻¹); 1605, 1492, 1463, 1443 (C–C in Ar, 1600–1585, 1500–1400 cm⁻¹); 1300, 1264, 1239 (C–N in Ar, 1335–1250 cm⁻¹); 1195, 1166, 1127 (C–O–C, 1250–1050 cm⁻¹); 807, 762, 697 (C–H in Ar, 900–675 cm⁻¹) cm⁻¹. EI-MS *m/z* 695.3751 (M⁺) (calcd 695.3763). Anal. Calcd for C₅₀H₄₉NO₂ (%): C 86.29, H 7.10, N 2.01, O 4.60. Found (%): C 86.21, H 7.16, N 2.06.

2,7-Bis(2,2-diphenylethenyl)-9-(2-ethylhexyl)-3,6-dimethoxycarbazole (3b). It was synthesized by the similar procedure as compound **3a** using 9-(2-ethylhexyl)-3,6-dimethoxycarbazole (**2b**, 0.50 g, 1.47 mmol), diphenylacetaldehyde (0.69 g, 3.53 mmol), (rac)-camphor-10-sulfonic acid (0.41 g, 1.767 mmol) and 5 ml of toluene. The residue was purified by silica-gel column chromatography using the mixture of hexane and ethyl acetate (20:1) as the eluent and recrystallized from hexane. The yield of yellow crystals was 31 % (0.32 g, FW = 695 g/mol, m.p.: 144–145 °C). ¹H NMR (400 MHz, CDCl₃) δ 7.32 – 7.16 (m, 24H), 6.59 (s, 2H), 3.89

(s, 6H), 3.19 – 3.07 (m, 2H), 1.53 – 1.47 (m, 1H), 1.14 – 1.05 (m, 3H), 0.97 – 0.87 (m, 3H), 0.79 (t, *J* = 7.3 Hz, 3H), 0.71 – 0.64 (m, 2H), 0.52 (t, *J* = 7.3 Hz, 3H). ¹³C NMR (100 MHz, CDCl₃, δ, ppm): 152.1, 144.0, 141.8, 141.2, 136.2, 130.8, 128.8, 128.2, 128.0, 127.4, 127.2, 125.5, 124.3, 121.6, 110.8, 101.0, 56.5, 47.4, 38.5, 30.6, 28.4, 27.1, 24.0, 23.4, 14.3, 10.9. *v*_{max} (KBr): 3077, 3054, 3021 (arene C–H, 3100–3000 cm⁻¹); 2954, 2930, 2870, 2858 (aliphatic C–H, 3000–2850 cm⁻¹); 1597, 1490, 1470, 1429 (C–C in Ar, 1600–1585, 1500–1400 cm⁻¹); 1310, 1269 (C–N in Ar, 1335–1250 cm⁻¹); 1201, 1160, 1063 (C–O–C, 1250–1050 cm⁻¹); 823, 774, 764, 696 (C–H in Ar, 900–675 cm⁻¹) cm⁻¹. EI-MS *m/z* 695.3740 (M⁺) (calcd 695.3763). Found (%): C 86.19, H 7.17, N 2.08.

The structures of **3a–b** were also proven by X-ray crystallography. The single-crystal of **3a** suitable for X-ray diffraction was grown from dilute hexane/THF solution while the crystal for **3b** was grown from the dilute methanol/THF solution at the room temperature. Crystal visualization and analysis were conducted using Mercury 3.3. Crystallographic data for compounds **3a** and **3b** are stored in open-access collection of crystal structures database in the Cambridge Crystallographic Data Centre with the following numbers: 1042467 and 1042468. These data can be obtained via www.ccdc.cam.ac.uk/data_request/cif, or by emailing data_request@ccdc.cam.ac.uk, or by contacting The Cambridge Crystallographic Data Centre, 12, Union Road, Cambridge CB2 1EZ, UK; fax: +4 4 1223 336033

Conclusions

2,7-Dimethoxy and 3,6-dimethoxy carbazole derivatives possessing diphenylethenyl moieties (**3a–b**) were synthesized by condensation of the corresponding derivative of dimethoxycarbazole (**2a–b**) with diphenylacetaldehyde. The structures of the synthesized compounds were proven by X-ray crystallography. Both of the isomers exhibit high thermal stability and form molecular glasses. Since the majority of molecules in crystal structure of **3a** form *J*-aggregates, this compound showed the effect of aggregation induced emission, while the other isomer, i.e. **3b**, showed the effect of aggregation-caused quenching. Both target compounds (**3a–b**) showed comparable ionization potentials of ca. 5.4 eV, which are lower compared to those of the parent dimethoxycarbazoles (**2a–b**). The derivative **3b** showed superior charge transporting properties relative to its counterpart **3a**. The time-of-flight hole drift mobilities in its amorphous layers exceeded 10⁻³ cm²/Vs at high electric fields. The pronounced differences in charge carrier mobility, thermal and optical properties were justified by the theoretical study using DFT and TD-DFT calculations. According to them, the target molecules of **3a** were found to be highly polar with the ground state dipole moment of 5.98 D, in contrast to the molecules of **3b** having the ground state dipole moment of ca. 0.69 D. The polarity was shown to a crucial effect on the molecular arrangement in the crystals, consequently on the thermal transitions (polymorphism) and on the charge-transporting properties of the isomers.

Acknowledgements

This work has been financially supported by the Taiwan-Latvia-Lithuania cooperation project "Synthesis and studies of organic electroactive materials for effective and reliable optoelectronic devices" (Latvia IZM No. 11-13/IZM 13-2, Lithuania TAPLLT1/13). Nataliya Kostiv acknowledges European Union Structural Funds project "Postdoctoral

Fellowship Implementation in Lithuania” for the financial support.

Notes and references

^a Department of Polymer chemistry and Technology, Kaunas University of Technology, Radvilenu St. 19, LT-50254 Kaunas, Lithuania.

^b Department of Solid State Electronics, Vilnius University, Sauletekio St. 9, LT-10222 Vilnius, Lithuania.

^c Institute of Solid State Physics, University of Latvia, 8 Kengaraga St., Riga LV-1063, Latvia

* Corresponding author: Juozas V. Grazulevicius; tel.: +370 37 300193; fax: +370 37 300152; e-mail: juozas.grazulevicius@ktu.lt

1. K. Müllen, U. Scherf, *Organic Light-Emitting Devices*, Wiley-VCH, Heidelberg, 2005, p. 410.
2. (a) C. D. Dimitrakopoulos and P.R. L. Malenfant, *Adv. Mater.*, 2002, **14**, 99–117. (b) M. Reig, J. Puigdollers and D. Velasco, *J. Mater. Chem. C*, 2015, **3**, 506.
3. (a) G. Puckyte, B. Schmaltz, A. Tomkeviciene, M. Degbia, J. V. Grazulevicius, H. Melhem, J. Bouclé and F. Tran-Van, *J. Power Sources*, 2013, **233**, 86. (b) P.-L. T. Boudreaux, S. Beaupré and M. Leclerc, *Polym. Chem.*, 2010, **1**, 127.
4. X. Guo, M. Baumgarten and K. Müllen, *Prog. Polym. Sci.*, 2013, **38**, 1832.
5. (a) J.-F. Morin, M. Leclerc, D. Adés and A. Siove, *Macromol. Rapid Commun.*, 2005, **26**, 761. (b) J. V. Grazulevicius, P. Strohriegl, J. Pielichowski and K. Pielichowski, *Prog. Polym. Sci.*, 2003, **28**, 1297.
6. G. Zotti, G. Schiavon, S. Zecchin, J.-F. Morin and M. Leclerc, *Macromolecules*, 2002, **35**, 2122.
7. F. Dierschke, A. C. Grimsdale and K. Müllen, *Synthesis*, 2003, **16**, 2470.
8. A. Tomkeviciene, J. V. Grazulevicius, K. Kazlauskas, A. Gruodis, S. Jursenas, T.-H. Ke and C.-C. Wu, *J. Phys. Chem. C*, 2011, **115**, 4887.
9. F.-I. Wu, P.-I. Shih, M.-C. Yuan, A. K. Dixit, C.-F. Shu, Z.-M. Chung and E. W.-G. Diau, *J. Mater. Chem.*, 2005, **15**, 4753.
10. T.-T. Wang, S.-M. Chung, F.-I. Wu, C.-F. Shu and E. W.-G. Diau, *J. Phys. Chem. B*, 2005, **109**, 23827.
11. J. H. Pan, Y. M. Chou, H. L. Chiu and B. C. Wang, *Aust. J. Chem.*, 2009, **62**, 483.
12. A. Sakalyte, J. Simokaitiene, A. Tomkeviciene, J. Keruckas, G. Buika, J. V. Grazulevicius, V. Jankauskas, C.-P. Hsu and C.-H. Yang, *J. Phys. Chem. C*, 2011, **115**, 4856.
13. J. Keruckas, R. Lygaitis, J. Simokaitiene, J. V. Grazulevicius, V. Jankauskas and G. Sini, *J. Mater. Chem.*, 2012, **22**, 3015.
14. H. Aziz and Z. D. Popovic, *Chem. Mater.*, 2004, **16**, 4522.
15. F. Li, K. G. Yager, N. M. Dawson, Y.-B. Jiang, K. J. Malloy and Y. Qin, *Chem. Mater.*, 2014, **26**, 3747.
16. F. Li, K. G. Yager, N. M. Dawson, J. Yang, K. J. Malloy and Y. Qin, *Macromolecules*, 2013, **46**, 9021.
17. F. Li, K. G. Yager, N. M. Dawson, Y.-B. Jiang, K. J. Malloy and Y. Qin, *Polym. Chem.*, 2015, **6**, 721.
18. J. Qu, Y. Suzuki, M. Shiotsuki, F. Sanda and T. Masuda, *Polymer*, 2007, **48**, 4628.
19. A. Dobarro, D. Velasco, V. v. Arnim and H. Finkelmann, *Macromol. Chem. Phys.*, 1997, **198**, 2563.
20. A. W. Freeman, M. Urvoy and M. E. Criswell, *J. Org. Chem.*, 2005, **70**, 5014.
21. H. Meng, Z.-K. Chen, X.-L. Liu, Y.-H. Lai, S.-J. Chua and W. Huang, *Phys. Chem. Chem. Phys.*, 1999, **1**, 3123.
22. J.C Li, Meng, Q.B. Meng, J. S. Kim, Y.S. Lee, *B. Kor. Chem. Soc.* 2009, **30**, 951.
23. Y. Kikugawa, Y. Aoki and T. Sakamoto, *J. Org. Chem.*, 2001, **66**, 8612.
24. G. Bubniene, T. Malinauskas, M. Daskeviciene, V. Jankauskas and V. Getautis, *Tetrahedron*, 2010, **66**, 3199.
25. W. Ishikawa, H. Inada, H. Nakano, Y. Shirota, *J. Phys. D: Appl. Phys.* 1993, **26**, 694.
26. L. Yu, G. A. Stephenson, C. A. Mitchell, C. A. Bunnell, S. V. Snorek, J. J. Bowyer, T. B. Borchardt, J. G. Stowell and S. R. Byrn, *J. Am. Chem. Soc.*, 2000, **122**, 585.
27. M. Sonntag and P. Strohriegl, *Chem. Mater.*, 2004, **16**, 4736.
28. G. Duvanel, J. Grilj, H. Chaumeil, P. Jacques and E. Vauthey, *Photochem. Photobiol. Sci.*, 2010, **9**, 908.
29. J. Morais, J. Ma and M. B. Zimmt, *J. Phys. Chem.*, 1991, **95**, 3885.
30. J. Mei, Y. Hong, J. W. Y. Lam, A. Qin, Y. Tang and B. Z. Tang, *Adv. Mater.*, 2014, **26**, 5429.
31. Y. Yang, X. Su, C. N. Carroll and I. Aprahamian, *Chem. Sci.*, 2012, **3**, 610.
32. F. Würthner, T. E. Kaiser and C. R. Saha-Möller, *Angew. Chem. Int. Ed.*, 2011, **50**, 3376.
33. J. R. Platt, *J. Chem. Phys.* 1949, **17**, 484.
34. J. T. Yi, L. Alvarez-Valtierra and D. W. Pratt, *J. Chem. Phys.*, 2006, **124**, 244302.
35. B. Zelent, T. Ganguly, L. Farmer, D. Gravel and G. Durocher, *J. Photochem. Photobiol. A*, 1991, **56**, 165.
36. J. L. Brédas, R. Silbey, D. S. Boudreaux and R. R. Chance, *J. Am. Chem. Soc.*, 1983, **105**, 6555.
37. J.F. Ambrose, R.F. Nelson, *J. Electrochem. Soc.* 1968, **115**, 1159.
38. B. W. D'Andrade, S. Datta, S. R. Forrest, P. Djurovich, E. Polikarpov and M. E. Thompson, *Org. Electron.*, 2005, **6**, 11.
39. R. Stanionyte, G. Buika, J. V. Grazulevicius and S. Grigalevicius, *Polym. Int.*, 2008, **57**, 1036.
40. P.M. Borsenberger, D.S. Weiss, *Organic photoreceptors for xerography*. New York: Dekker; 1998. p. 768.
41. Z. Shuai, L. Wang, C. Song, *Theory of Charge Transport in Carbon Electronic Materials*, SpringerBriefs in Molecular Science, Springer, 2012.
42. A. Wakamiya, H. Nishimura, T. Fukushima, F. Suzuki, A. Saeki, S. Seki, I. Osaka, T. Sasamori, M. Murata, Y. Murata and H. Kaji, *Angew. Chem. Int. Ed.*, 2014, **53**, 5800.
43. V. Coropceanu, J. Cornil, D. A. da Silva Filho, Y. Olivier, R. Silbey and J.-L. Brédas, *Chem. Rev.*, 2007, **107**, 926.
44. W.-C. Chen and I. Chao, *J. Phys. Chem. C*, 2014, **118**, 20176.
45. S. Duhm, Q. Xin, S. Hosoumi, H. Fukagawa, K. Sato, N. Ueno and S. Kera, *Adv. Mater.*, 2012, **24**, 901.
46. N. Sato, H. Inokuchi, E. A. Silinsh, *Chem. Phys.*, 1987, **115**, 269–277.
47. J. E. Norton and J.-L. Brédas, *J. Am. Chem. Soc.*, 2008, **130**, 12377.
48. S. M. Ryno, S. R. Lee, J. S. Sears, C. Risko and J.-L. Brédas, *J. Phys. Chem. C*, 2013, **117**, 13853.
49. M. Malagoli and J. L. Brédas, *Chem. Phys. Lett.*, 2000, **327**, 13.
50. E. F. Valeev, V. Coropceanu, D. A. da Silva Filho, S. Salman and J.-L. Brédas, *J. Am. Chem. Soc.*, 2006, **128**, 9882.
51. J.-D. Chai and M. Head-Gordon, *Phys. Chem. Chem. Phys.*, 2008, **10**, 6615.
52. Spartan'14 for Windows Version 1.1.2. 1840 Von Karman Avenue, Suite 370, Irvine, CA.
53. L. B. Schein and A. R. McGhie, *Phys. Rev. B*, 1979, **20**, 1631.
54. M. Kasha, H. R. Rawls, M. Ashraf El-Bayoumi, *Pure Appl Chem.*, 1965, **11**, 371.
55. A. Goonesekera and S. Ducharme, *J. Appl. Phys.*, 1999, **85**, 6506.
56. A. Dieckmann, H. Bässler and P. M. Borsenberger, *J. Chem. Phys.*, 1993, **99**, 8136.
57. C. F. Macrae, I. J. Bruno, J. A. Chisholm, P. R. Edgington, P. McCabe, E. Pidcock, L. Rodriguez-Monge, R. Taylor, J. van de Streek and P. A. Wood, *J. Appl. Crystallogr.*, 2008, **41**, 466.
58. T. Malinauskas, M. Daskeviciene, K. Kazlauskas, H.-C. Su, J. V. Grazulevicius, S. Jursenas, C.-C. Wu and V. Getautis, *Tetrahedron*, 2011, **67**, 1852.
59. G. Blazys, S. Grigalevicius, J. V. Grazulevicius, V. Gaidelis, V. Jankauskas and V. Kampars, *J. Photochem. Photobiol. A*, 2005, **174**, 1.
60. E. Miyamoto, Y. Yamaguchi, M. Yokoyama, *Electrophotography*, 1989, **28**, 364.
61. E. Montrimas, V. Gaidelis, A. Pazera, *Lithuanian J. Phys.* 1966, **6**, 569.
62. S.M.Vaezi-Nejad, *Int. J. Electron.* 1987, **62**, 361.
63. C. A. Amorim, M. R. Cavallari, G. Santos, F. J. Fonseca, A. M. Andrade and S. Mergulhão, *J. Non-Cryst. Solids*, 2012, **358**, 484.
64. Gaussian 09, Revision A.02, Gaussian, Inc., Wallingford CT, 2009.